

# CHARACTERISTICS OF THE THERMAL FATIGUE RESISTANCE FOR 3.1C, 0.8Si, 0.9Mn, 1.7Cr, 4.5Ni AND 0.3Mo ICDP CAST IRON ROLL AT 600 °C

## ZNAČILNOSTI ODPORNOSTI ZLITIN LITEGA ŽELEZA ZA VALJE 3.1C, 0.8Si, 0.9Mn, 1.7Cr, 4.5Ni IN 0.3Mo NA ICDP TERMIČNO UTRUJANJE PRI 600 °C

Milan Terčelj<sup>1</sup>, Peter Fajfar<sup>1</sup>, Matjaž Godec<sup>2</sup>, Goran Kugler<sup>1</sup>

<sup>1</sup>University of Ljubljana, Faculty of Natural Science and Engineering, 12 Aškerčeva street, 1000 Ljubljana, Slovenia

<sup>2</sup>Institute of Metals and Technology, Lepi pot 11, 1000 Ljubljana, Slovenia  
Goran.Kugler@omm.ntf.uni-lj.si

Prejem rokopisa – received: 2016-08-23; sprejem za objavo – accepted for publication: 2016-08-31

doi:10.17222/mit.2016.259

Using a new test rig the characteristics related to the thermal fatigue resistance for ICDP (Indefinite Chill Double Pour) cast iron for hot working rolls was investigated. Tests were carried out at 600 °C to obtain the characteristics of cracks at (500, 1000 and 1500) cycles. For comparative purposes, additionally a test at 500 °C was carried out. The average length of all the cracks, their density, average length of five longest cracks and relevant microstructural characteristics for the mentioned cycles were determined. It was found that the cracks initiation and their growth are related to the cracking and spalling of the carbides, shape of graphite, distribution of carbides and graphite particles, oxidation, etc. The obtained results contribute to a better understanding of the thermal cracking of selected roll cast iron. Based on these results the suggestions for improving the thermal fatigue resistance for the cast iron roll are given.

Keywords: roll cast iron, thermal fatigue, cementite, graphite, cracks

Novo razvita naprava je bila uporabljena za raziskave lastnosti ICDP litega železa, ki so povezane z odpornostjo na termično utrujanjem. Značilnosti razpok so bile določene po (500, 1000 in 1500) ciklih, pri 600 °C. Za primerjavo je bilo izvedenih nekaj testiranj tudi pri 500 °C. Na osnovi rezultatov testiranj je bilo za vsako število ciklov določena povprečna dolžina vseh dobljenih razpok, njihova gostota, povprečna dolžina petih najdaljših razpok, vključno z ostalimi relevantnimi mikrostrukturnimi značilnostmi. Rezultati so pokazali, da sta nukleacija in rast razpok tesno povezana s pokanjem in drobljenjem karbidov, z geometrijo grafita, z volumsko porazdelitvijo karbidov ter grafitnih delcev, z oksidacijo, itd. Rezultati prispevajo k boljšemu razumevanju termičnega pokanja izbranega materiala za valje. Na osnovi predstavljenih rezultatov so podani predlogi za izboljšanje odpornosti litega železa za valje na termično utrujanje.

Ključne besede: lito železo za valje, termično utrujanje, cementit, grafit, razpoke

## 1 INTRODUCTION

Dies used in hot-working applications like die casting, rolling, forging and hot extrusion are exposed to high thermal, mechanical, tribological and chemical loads. The occurrence of different damage, i.e., cracks, fracture, plastic deformation and wear, are a consequence of the different magnitudes of the mentioned loads as well as their different mutual ratios, materials properties, etc.<sup>1–7</sup> Thus, in the case of cyclical subjection to high temperatures, i.e., the heating of rolls (also above 600 °C) and their water cooling, these conditions lead to the occurrence of cracking on the die's surface, which appears in the shape of a crack network that consequently results in spalling of the die material that further leads to a deterioration of the surface finish of the workpiece. In hot-working rolls the thermal stresses are usually comparable or even larger than the mechanical stresses.<sup>3–10</sup>

To increase the die's service time it is important and also the common task for both die designers as well as for producers of die steels, to shift the occurrence of

cracks to later times and to decrease their growth rate. Hot working rolls are usually alloyed with Cr, V, Mo, W, and after solidification process they are heat treated accordingly. Furthermore, with optimization of the chemical composition and the process parameters of the roll production improved microstructure with better thermal fatigue resistance for each individual application can be achieved. In relation to the desired microstructural properties it is important to achieve (i) appropriate type, size, amount, shape, distribution, etc. of carbides, (ii) amount, size and shape of graphite particles, (iii) grain size, etc. Thus, regarding the specific application the appropriate combination of mechanical (ductility, yield strength, toughness, hardness, etc.), thermal, microstructural properties as well as oxidation resistance should be engineered.<sup>3–17</sup>

Several research works related to thermal fatigue resistance of die materials (i.e. steels, cast irons) were carried out where reasons for initiation and growth of cracks at hot working dies (forging, die casting)<sup>17–30</sup> and hot working rolls<sup>3–6,9,31–34</sup> were investigated using various

laboratory tests. However, detailed knowledge about the influence of the stress state, the temperature and the oxidation on the initiation and propagation of thermal cracks in hot working applications is still lacking. Each of the applied laboratory tests has some advantages and disadvantages from the point of view of achieving of test conditions and their controllability. Thus, the accuracy of achieving the prescribed test temperature and subsequent cooling rate are key factors that influence the quality of the obtained laboratory results and consequently also on an explanation of the crack initiation and their growth.<sup>19–27</sup>

In this work the thermal fatigue resistance of Indefinite Chilled Double Poured (ICDP) cast iron for rolls at two different temperatures was studied using a new test rig with specially prepared test samples. The resistance to thermal fatigue at three different numbers of heating-cooling cycles were evaluated by measuring the average length of cracks, their density, average length of five largest cracks and the relevant microstructures. The initiation and growth of the cracks were evaluated and explained. Some suggestions for improvement of thermal fatigue resistance for the used cast iron roll are given.

## 2 EXPERIMENTAL PART

### 2.1 ICDP cast iron

ICDP cast iron with the chemical composition given in **Table 1** was used for thermal fatigue testing. From the table it is clear that there is an increased content of C (above 3 %) as well as for Si, Mn, Cr, Mo in comparison to the usual constructional steels and almost 4.5 %Ni. Thus, due to high content of carbon as well as the presence of carbide-forming elements, i.e., Cr, Mo and V, this indicates the presence of carbides and graphite in the microstructure.

**Table 1:** Chemical composition of used cast iron in mass fraction, (w/%)

**Tabela 1:** Kemijska sestava uporabljenega litega železa v masnih deležih, (w/%)

C	Si	Mn	Cr	Ni	Mo	V	W	Nb
3.11	0.84	0.86	1.71	4.45	0.30	0.13	0.01	0.01

### 2.2 Applied thermal fatigue test and conditions of testing

The shape of the samples and the applied thermal fatigue tests are shown in **Figures 1a** and **1b**, respectively. Hollow specimen is on both sides tightly clamped between two copper anvils which are placed in the working cells of a Gleeble 1500D thermo-mechanical simulator. On the middle of 12 mm working length of samples thermocouple wires of type K are welded, while water and air inlet as well as their outlet from samples are enabled by tubes fixed on its both lateral sides. Heating of the specimen and its cooling by water and air

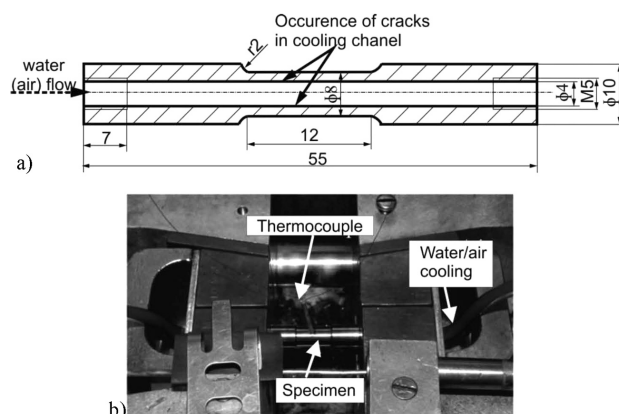


**Figure 1:** a) Used sample for thermal fatigue test and b) tight clamped sample between two copper anvils in working cells of the Gleeble 1500D

**Slika 1:** a) Vzorec za testiranje termičnega utrujanja, b) tesno vpetje med dvoje čeljusti iz bakra v delovni celici naprave Gleeble 1500D

that flow through hollow specimen is computer guided, whereas constant testing conditions, i.e., achieving of constant heating to test temperature and specimen internal cooling, are ensured (**Figure 2**). Regarding the program the specimens were heated to a selected temperature in 3 s, which was followed by water cooling and emptying of specimen by air flow. Thus, the temperature gradient and consequently the stress gradient on the internal surface of the specimen is achieved. On this area (**Figure 1a**) the occurrence of cracks is expected. A maximum selected test temperature was 600 °C and for comparative reason also test at 500 °C was carried out. At test temperature of 600 °C cracks were observed and measured after 500, 1000 and 1500 thermal cooling cycles, while at 500 °C this was done after 1000 cycles (**Table 2**). After a selected number of cycles the working lengths of samples were cut in radial as well as in the axial directions. Characterization of the cracks was focused within area of 8 mm length of the central working dimension of samples. The cracks were characterized by (i) mean length of all cracks, (ii) density of cracks, i.e.,

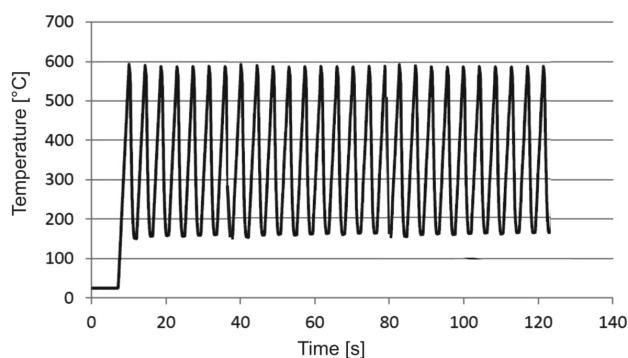


**Figure 2:** Measured time courses of temperature on outside surface of test specimen

**Slika 2:** Izmerjeni časovni potek temperature na zunanji površini vzorca za testiranje

average number of cracks per length of 1mm, and (iii) average length of the 5 longest cracks.

**Table 2:** Test conditions

**Tabela 2:** Pogoji testiranja

Test temperature	No. of cycles
500 °C	1000
600 °C	500, 1000, 1500

### 2.3 Characterization of cracks, carbides and microstructure

Optical microscopy (OM, Carl Zeiss AXIO Imager A1m) and a field-emission scanning electron microscope (FE SEM JEOL 6500F) in combination with the attached Energy-Dispersive Spectroscopy (EDS, INCA x-SIGHT LN2 with INCA ENERGY 450 software) analytical tool were applied for observations of microstructure, i.e., determination of main constituents (graphite, cementite (carbides), etc.), characterization of cracks, etc. Furthermore, the amount of cementite (carbides) as well as of graphite particles regarding to size, distribution and shape were determined. Thus by means of automatic image analysis the form, distribution, and size of graphite nodes were classified according to the EN ISO 945 standard. The specimens used in optical microscopy were etched with 3 % Nital reagent.

## 3 RESULTS

### 3.1 Characterization of initial microstructure of cast iron

The obtained microstructure of the initial material at room temperature is presented in **Figure 3a** (OM) with details in **Figure 3b** as well as in **Figure 3c** (BEI) with mapping for C in **Figure 3d**. As can be seen the microstructure consists of martensite, retained austenite, carbides (cementite), graphite and also MnS inclusions. The results of the EDS analyses, which served for clear distinction between cementite and graphite, are given in **Table 3**. In general, cementite contains a considerably smaller amount of C in comparison to graphite. Thus, in cementite (carbides) besides C and Fe also main carbide-forming elements, i.e., Cr, Mo and V, as well as Co and Ni were found. The relative lower obtained values for C contents in cementite and graphite can be attributed to the detection depth of EDS analyses, whereas in our case this exceeded the depth of the interface between both relevant constituents and matrix, i.e., the

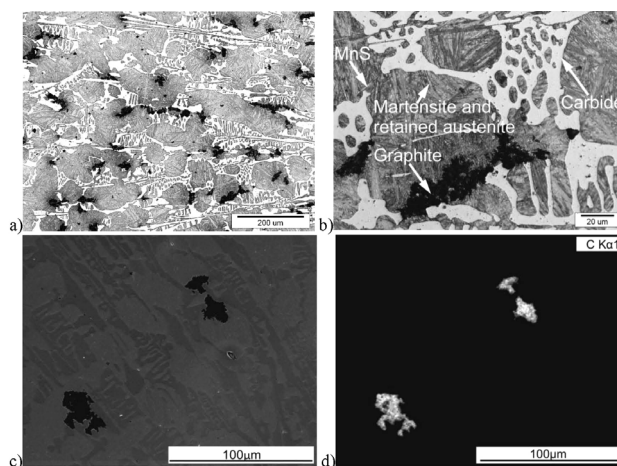


**Figure 3:** a) Initial microstructure (OM) of used cast iron with b) detail, c) BEI image showing carbides and graphite and d) corresponding X-ray image (mapping) of C distribution

**Slika 3:** Začetna mikrostruktura (OM) uporabljenega litega železa; a) z detajlom, b) slika BEI, ki prikazuje karbide in grafit, c) pripadajoča XRD slika (mapiranje), d) porazdelitev ogljika

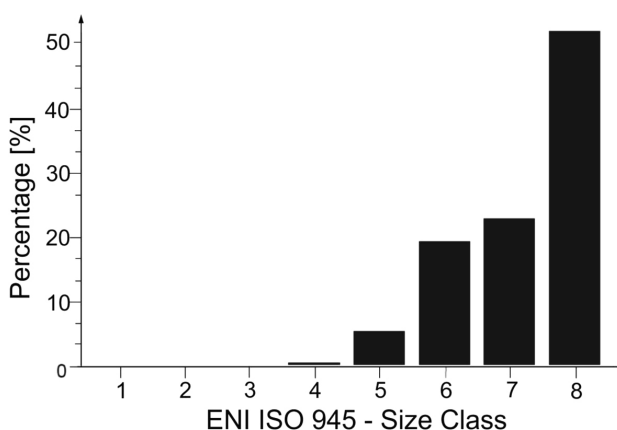


**Figure 4:** Percentage of graphite particles regarding their size

**Slika 4:** Delež grafitnih delcev v povezavi z njihovo velikostjo

matrix was also partly included in the analyses that apparently detected lower C contents. Furthermore, it is also known that EDS analysis for light elements is not a very accurate method. A SEI image of the initial microstructure is given in **Figure 3c**, while the distribution of carbon is given in **Figure 3d**. Thus, also by this graphite particles and cementite can be clearly distinguished. Note that the obtained microstructure is very similar to the microstructure found in 45 for cast iron for rolls with similar chemical composition.

**Table 3:** EDS analyse of chemical elements in carbides, graphite and martensite of used cast iron in mass fractions, (w%)

**Tabela 3:** EDS-analiza kemičnih elementov v karbidih, grafitu ter martenzitu za uporabljeno lito železo v masnih deležih, (w%)

	C	Si	Mn	Cr	Mo	V	Co	Ni	Fe	O	Al	Imp.
Carbides	5.7		0.9	3.6	0.3	0.3	1.3	1.8	91.4			rest
Graphite	93.9	-	-	-	-	-	-	-	6.1	-	-	-
Martensite	2.5	1.2	0.6	0.5	-	-	-	5.4	89.7	-	-	rest

The percentage of graphite and carbides in the microstructure amounted approximately 4.9 % and 29.5 %, respectively, where the nodularity of the graphite was 0.34. Using automatic image analysis, the form, distribution, and size of graphite nodes were classified according to the EN ISO 945 standard. The majority (almost 60 %) of the graphite particles were of Form II (crab or spiky) or (15 %) of Form III (vermicular) (**Figure 4**). More than half of all the graphite particles were smaller than 15  $\mu\text{m}$ , equivalent to size class 8 (**Figure 4**).

### 3.2 Characterization of cracks growth

As mentioned above the obtained characteristics of cracks refer to the length of 8 mm in central working length of the samples. Numbers of cracks for different class length of cracks in dependence on number of cycles and for test temperature of 600  $^{\circ}\text{C}$  are given in **Figure 5**. As can be seen, in general, the number of cracks decreases with increasing of class length for all numbers of cycles. Thus, for the class length of cracks up to 100  $\mu\text{m}$  the number of cracks amounts about 70 for all number of cycles, at class length range 100–200  $\mu\text{m}$  this value amounts slightly below 20, while at class length range 200–300  $\mu\text{m}$  the number of cracks is in the range 3–6. With further increasing of class length range the number of cracks decreases, thus in class length range 800–900  $\mu\text{m}$  only one crack for thermal cycle 1000 and 1500, respectively, were obtained.

For the comparison at 1000 cycles and 500  $^{\circ}\text{C}$  the number of cracks are up to class length range of 300  $\mu\text{m}$ , approximately by about 20 % lower in comparison to the test temperature of 600  $^{\circ}\text{C}$  and the same number of thermal cycles. Furthermore, the longest cracks at test temperature of 500  $^{\circ}\text{C}$  and 1000 thermal cycles were about 500  $\mu\text{m}$ .

From **Figure 6a** it is clear that at test temperature of 600  $^{\circ}\text{C}$  the average lengths of all the cracks increases with the number of cycles. Thus, after 500 thermal

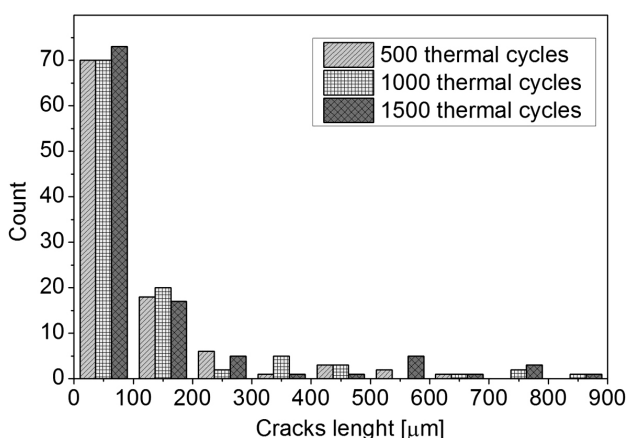


**Figure 5:** Distribution of crack number related to class length and in dependence on number of thermal cycles and test temperature

**Slika 5:** Porazdelitev števila razpok v povezavi z razredom dolžin v odvisnosti od števila termičnih ciklov ter temperature testiranja

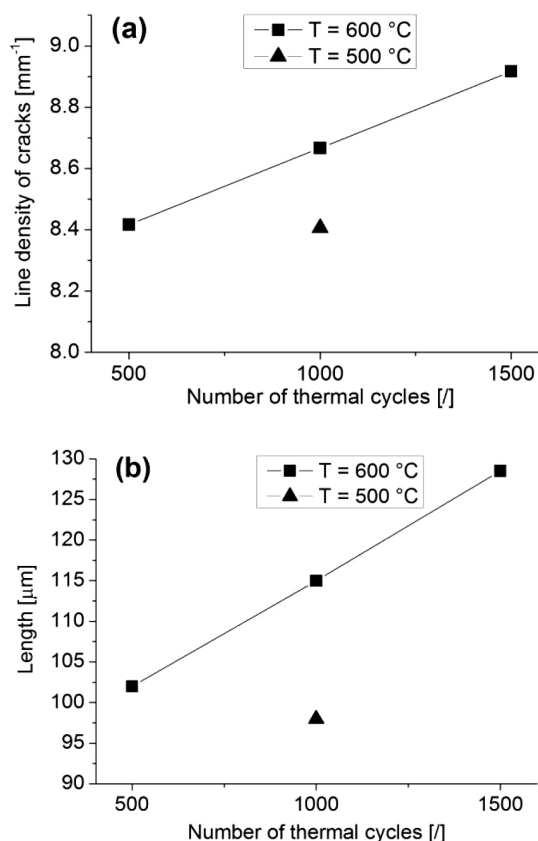


**Figure 6:** a) Average lengths of all cracks and b) cracks density in dependence of the number of thermal cycles and test temperature  
**Slika 6:** a) Povprečna velikost vseh razpok b) in gostota razpok kot funkcija števila termičnih ciklov in temperature testiranja

cycles the average crack length amounts to 102  $\mu\text{m}$ , at 1000 cycles, 115  $\mu\text{m}$  and at 1500 cycles, 127  $\mu\text{m}$ . For comparative test conditions, i.e., 500  $^{\circ}\text{C}$  and 1000 cycles, the average crack length amounted to 97  $\mu\text{m}$ . As expected, this value is lower in comparison to the one obtained for a temperature of 600  $^{\circ}\text{C}$  for the same thermal cycles. Similar relationships were also obtained for the crack density, which is shown in **Figure 6b**. Thus at the test temperature of 500  $^{\circ}\text{C}$  and 1000 cycles the density of cracks was 8.4 cracks/mm, i.e., lower in comparison to the test temperature of 600  $^{\circ}\text{C}$  and the same number of cycles where this value was 8.7 cracks/mm. At 500 cycles and the same temperature this value is slightly lower, i.e., 8.4 cracks/mm, while at 1500 cycles it is slightly higher, i.e., 8.9 cracks/mm, regarding to 1000 cycles. Therefore, the density of the cracks increases only slightly with the increasing number of cycles and decreases with lower test temperature. The lower density of cracks at the lower temperature can be attributed to the lower stresses on the tested surface layer.

Also, the average length of the five longest cracks at test temperature of 600  $^{\circ}\text{C}$  increases with the number of cycles (**Figure 7**). Thus, this value is 570  $\mu\text{m}$  at 500 cycles, 700  $\mu\text{m}$  at 1000 cycles and 840  $\mu\text{m}$  at 1500

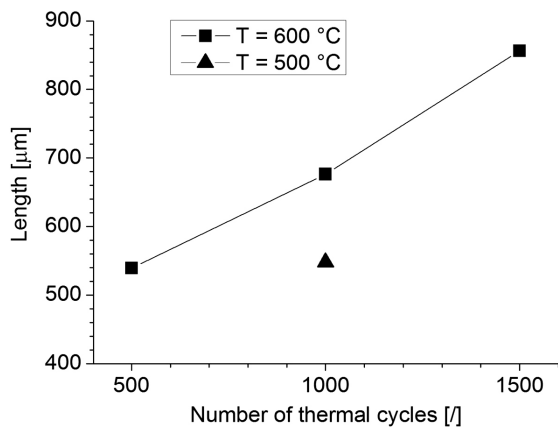


**Figure 7:** Average lengths of five longest cracks in dependence of the number of thermal cycles and test temperature

**Slika 7:** Povprečna velikost petih najdaljših razpok kot funkcija števila termičnih ciklov in temperature testiranja

cycles. For comparison, this value at the temperature of 500 °C and 1000 cycles was expectedly lower and is about 540  $\mu\text{m}$ .

### 3.3 Microstructural characteristics of cracks

Cracks were predominately initiated at spots on the tested surface where the carbides are present (Figures 8a to 8b). This process, which is a consequence of tensile stresses on surface layer, begins with cracking and spalling of the carbides, where cracks grow along the carbides, i.e., they use the carbides path. Figure 8b shows an empty area as a consequence of the carbides spalling at the crack’s origin. Namely, the carbides have a lower temperature expansion coefficient and are also more brittle in comparison to the matrix. Thus during heating and cooling they cannot fully follow the dilatation of the base material and consequently they represent a notch effect, i.e., stress concentration. Furthermore,

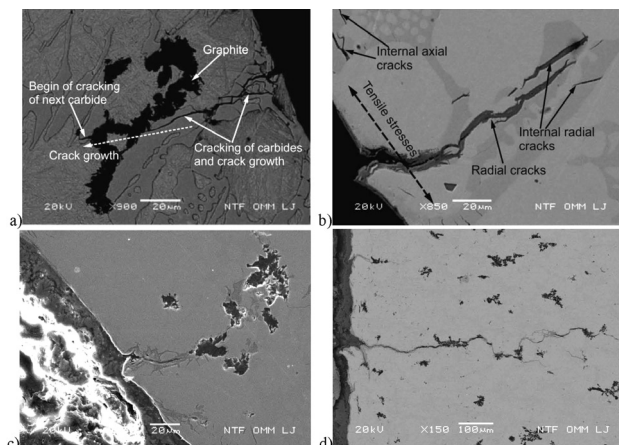


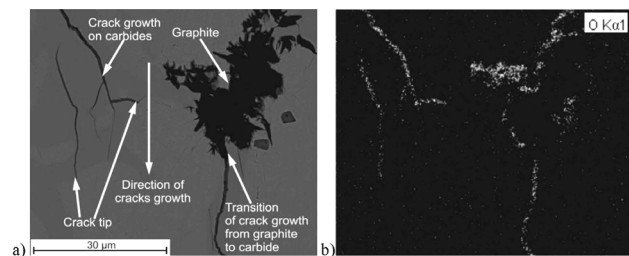
**Figure 8:** a) Initiation of cracks and cracking of carbides and b) growth of cracks using carbides (cementite) path, (c–d) growth of cracks using carbides and graphite particles

**Slika 8:** a) Nukleacija razpok ter pokanje karbidov in b) rast razpok po karbidnih (cementitnih) poteh, (c–d) rast razpok preko karbidov in grafitnih delcev

from Figure 8b it is also clear that the crack ends at the carbide–matrix interface. Note that crack growth within the matrix is hindered. In Figure 8b micro-cracks are visible that do not originate from the cooled surface but are internal in nature and are oriented in radial as well as in axial directions. EDS analyses revealed oxidation that expands on both sides of the crack.

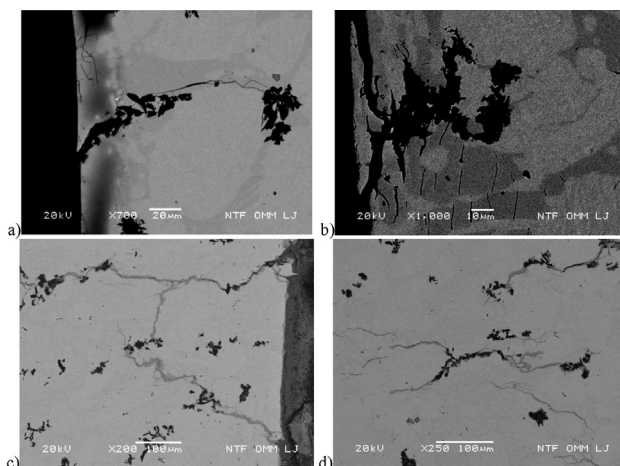
In Figure 8a it can be also seen the transition of cracks growth from carbide to graphite and again to carbide, where crack again finishes at the carbide–matrix interface. This case illustrates alternating of carbide and graphite at crack growth that is also presented in Figures 8c to 8d. It should be emphasized here that the shape of the carbides plays an important role since cracks usually grow in the direction of the flattened shaped graphite where the stress intensity is increased. Thus, nodularity (in this case 0.34) of the graphite should be increased in order to decrease the growth rates of the cracks. Similar results were also obtained by X. Tong et al.,<sup>18</sup> i.e., the thermal fatigue resistance of samples made from cast iron were sorted as nodular graphite iron > vermicular graphite iron > flake graphite iron. Furthermore, since cracks grow through carbide–graphite paths, their growth would be decreased by the interruption of these paths. This can be done by adding rare-earth elements. Note that in this way Wang et al.<sup>31</sup> achieved coagulation of the carbides and graphite and consequently also better thermal fatigue resistance of the roll steel. It can be assumed that a similar approach could also contribute to improved fatigue resistance for our type of roll cast iron. Also, slight hot deformation of the working layer of rolls would probably act in similar way, i.e., interruption of carbides paths by crushing of carbides.

Figure 9a shows the growth of cracks using the carbide and graphite path, while in Figure 9b the distribution of oxygen is presented. From both figures it is clear that during crack growth oxidation has taken place. This is also visible at the crack tip that decreases the local strength properties of the matrix and consequently also accelerates the growth rate of the cracks. Furthermore, it is also clear that the cracks in the graphite do not grow through its central part but along both lateral sides.



**Figure 9:** a) Crack growth in carbides (cementite) and graphite and oxidation of cracks, b) distribution of oxygen in cracks internal and on crack tip

**Slika 9:** a) Rast razpok v karbidih (cementitu) in grafitu ter oksidacija razpok, b) porazdelitev kisika v notranjosti razpok ter v njenih konicah



**Figure 10:** a) Initiation of cracks at sharp shaped (formed) graphite, b) spalling of small sized part of matrix at graphite, c) unification (linking) of cracks originate from different initial spots at surface, d) internal crack extending carbides and graphite particles

**Slika 10:** a) Nukleacija razpok na ostri obliki grafita, b) drobljenje majhnih delov grafitne matrike, c) združevanje razpok, ki izvirajo iz različnih začetnih točk na površini, d) širjenje notranje razpoke med karbidi in grafitnimi delci

Further crack growth from the graphite to carbides is characterized by crack oxidation of the main crack and by the occurrence of new micro-cracks on both sides. Note that improvement of oxidation resistance also leads to an improvement of the thermal fatigue resistance.<sup>6,16,32</sup>

As already mentioned, cracks are usually initiated at the carbides on cooled surfaces, which is shown in **Figure 10a**. But in very limited cases they are also initiated at the sharp graphite particles that are elongated in the longitudinal direction, i.e., flattened graphite particles. Furthermore, since the graphite is softer than the matrix, this can also lead to a notch effect at such spots. Otherwise, it was found that for the more equiaxed graphite that precipitated at the cooled surface, cracks do not occur, since only spalling of the small-sized base material takes place, as presented in **Figure 10b**. From this figure it is also visible the occurrence of microcracks in the axial direction in carbides close to the graphite. This behaviour was very frequently observed and can be attributed to the differences in the thermal expansions of all the main constituents (i.e., matrix, carbides and graphite) leading to local bending of carbides as a consequence of the occurrence of the temperature gradient and the different thermal dilatation, i.e., outer regions are subjected to higher thermal dilatation. Moreover, in this case the carbides are oriented perpendicular to the cooled surface and the cracks appeared approximately in length area of the graphite particle.

Spalling of the material occurs also when cracks, which originate from different initial spots on cooled surface, unify (link) in one crack. Consequently, no adhesion between the base and the crack limited part of base material exists (**Figure 10c**). It was also observed that not only internal micro-cracks for which extension is

limited inside the carbides, but also connected internal cracks extend across several carbides and graphite particles (**Figure 10d**). Furthermore, in some cases graphite can hinder the crack growth when it is located far enough from the cooled surface and if its shape is approaching spherical.

## 4 CONCLUSIONS

Using a specially developed test rig, the resistance against thermal fatigue for ICDP cast iron roll was investigated. Tests were carried out at 500 °C and 600 °C and characteristics related to cracks at 500, 1000 and 1500 cycles were obtained. The average length of all the cracks, crack density, average length of five longest cracks and microstructure characteristics related to cracks were determined. From the results the following conclusions can be derived:

- Microstructure of tested cast iron consists of carbides (cementite), graphite particles, MnS inclusions which are inserted in the martensite matrix. Percentage of graphite with value for nodularity of 0.34 amounted 4.9 %, while percentage for carbides amounted 29.5 %.
- The initiation of cracks is predominately on spots of precipitated carbides on the cooled surface.
- In a very few cases also the initiation of cracks at graphite particles with thin (flattened) and elongated shape, was observed. In the case of location of spherical shaped graphite particles at cooled surface this results only in spalling of base material.
- Cracks grow using carbides (cementite) and graphite paths. Thin (flattened) and elongated shapes of graphite are more appropriate at cracks growth than spherical.
- Average length of all cracks as well as cracks density at test temperature of 600 °C increases almost linearly with an increasing of number of cycles.
- For 1000 cycles the density of the cracks at the test temperature of 500 °C was lower in comparison to the test temperature of 600 °C. The occurrence of oxidation within the cracks as well as at crack tips was revealed, which results in acceleration of crack growth.
- Decreasing the possibility of the connection of carbides and graphite cracks paths will decrease the growth rate of cracks. This could be achieved (i) by crushing of carbides cells, i.e., by imposing of hot plastic deformation, (ii) by refining of carbides by additional alloying by rare-earth elements<sup>31</sup>, (iii) by increasing nodularity of graphite and (iv) by improving the heat treatment as well as rolls production procedures.

## 5 REFERENCES

- <sup>1</sup> F. J. Belzunce, A. Ziadi, C. Rodriguez, Structural integrity of hot strip mill rolling rolls, *Engineering Failure Analysis*, 11 (2004), 789–797, doi:10.1016/j.engfailanal.2003.10.004
- <sup>2</sup> R. Colas, J. Ramirez, I. Sandoval, J. C. Morales, L. A. Leduc, Damage in hot rolling work rolls, *Wear* 230 (1999), 56–60, doi:10.1016/S0043-1648(99)00081-2
- <sup>3</sup> K. Goto, Y. Matsuda, K. Sakamoto, Y. Sugimoto, Basic Characteristics and Microstructure of High-carbon High Speed Steel Rolls for Hot Rolling Mill, *ISIJ Int.* 32 (1992), 1184–1189, doi:10.2355/isijinternational.32.1184
- <sup>4</sup> N. F. G. Montes de Oca, R. Colas, W. M. Rainfort, On the damage of work roll grade high speed steel by thermal cycling, *Engineering Failure Analysis*, 18 (2011), 1576–1583, doi:10.1016/j.engfailanal.2011.06.001
- <sup>5</sup> G. K. Ahiale, W. D. Choi, Y. Suh, Y. K. Lee, Y. J. Oh, Effect of MC-Type Carbide Forming and Graphitizing Elements on Thermal Fatigue Behaviour of Indefinite Chilled Cast Iron Rolls, *Metallurgical and Materials Transactions A*, 46A (2015), 4819–4827, doi:10.1007/s11661-015-3090-2
- <sup>6</sup> M. Yong-an, J. Bergström, W. Xiao-chun, X. Luo-ping, Oxidation and Thermal Fatigue Behaviors of Two Type Hot Work Steels During Thermal Cycling, *Journal of iron and steel research*, 20 (2013) 11, 90–97, doi:10.1016/S1006-706X(13)60202-2
- <sup>7</sup> B. Podgornik, V. Leskovšek, Wear mechanisms and surface engineering of forming tools, *Mater. Tehnol.*, 49 (2015) 3, 313–324, doi:10.17222/mit.2015.005
- <sup>8</sup> M. Sedlaček, B. Podgornik, S. Milanovič, A modified heat treatment to improve the properties of double layer cast rolls, *Mater. Tehnol.*, 48 (2014) 6, 983–990
- <sup>9</sup> C. K. Kim, J. I. Park, J. H. Ryu, S. Lee, Correlation of Microstructure and Thermal Fatigue Property of Centrifugally Cast High-Speed Steel Rolls, *Metallurgical and Materials Transactions A*, 35 (2004), 481–492, doi:10.1007/s11661-004-0359-2
- <sup>10</sup> V. Leskovšek, B. Podgornik, Multifunctional Kic test specimen for assessment of different tool and high speed steel properties, *Mater. Tehnol.*, 47 (2013) 3, 273–283
- <sup>11</sup> D. Mitrovič, P. Mrvar, M. Petrič, Characterization of cast-iron gradient castings, *Mater. Tehnol.*, 49 (2015) 6, 871–875, doi:10.17222/mit.2014.102
- <sup>12</sup> J. Gontarev, M. Doberšek, J. Medved, P. Mrvar, Solidification of hypereutectoid high speed steel for rolls, *Metallurgija* 50 (2011) 1, 29–32
- <sup>13</sup> M. Stürmera, J. Dagnerb, P. Manstetena, H. Köstler, Real-time simulation of temperature in hot rolling rolls, *Journal of Computational Science*, 5 (2014), 732–742, doi:10.1016/j.jocs.2014.04.003
- <sup>14</sup> D. Benasciuttia, E. Brusab, G. Bazzaroc, Finite elements prediction of thermal stresses in work roll of hot rolling mills, *Procedia Engineering*, 2 (2010), 707–716, doi:10.1016/j.proeng.2010.03.076
- <sup>15</sup> M. Pellizzari, A. Molinari, G. Straffelini, Tribological behaviour of hot rolling rolls, *Wear* 259 (2005), 1281–1289, doi:10.1016/j.wear.2004.12.006
- <sup>16</sup> A. Molinari, G. Straffelini, A. Tomasi, A. Biggi, G. Corbo, Oxidation behaviour of ledeburitic steels for hot rolls, *Materials Science and Engineering A*, 280 (2000) 255–262, doi:10.1016/S0921-5093(99)00693-0
- <sup>17</sup> M. Pellizzari, A. Molinari, G. Straffelini, Thermal fatigue resistance of gas and plasma nitrided 41CrAlMo7 steel, *Materials Science & Engineering A*, 352 (2003) 186–194, doi:10.1016/S0921-5093(02)00867-5
- <sup>18</sup> X. Tong, H. Zhou, L.-Q. Ren, Z.-H. Zhang, W. Zhang, R.-D. Cui, Effects of graphite shape on thermal fatigue resistance of cast iron with biomimetic non-smooth surface, *International Journal of Fatigue*, 31 (2009), 668–677, doi:10.1016/j.ijfatigue.2008.03.023
- <sup>19</sup> A. Persson, S. Hogmark, J. Bergström, Simulation and evaluation of thermal fatigue cracking of hot work tool steel, *International Journal of Fatigue*, 26 (2004), 1095–1107, doi:10.1016/j.ijfatigue.2004.03.005
- <sup>20</sup> M. Fazarinc, R. Turk, G. Kugler, P. Mrvar, M. Terčelj, Development of test rig for thermal fatigue testing: preliminary results, *RMZ - Materials and geoenvironment*, 54 (2007) 1, 38–48
- <sup>21</sup> S. Amiable, S. Chapuliot, A. Constantinescu, A. Fissolo, A comparison of life time prediction methods for a thermal fatigue experiment, *International Journal of Fatigue*, 28 (2006), 692–706, doi:10.1016/j.ijfatigue.2005.09.002
- <sup>22</sup> A. Fissolo, S. Amiable, O. Ancelet, F. Mermaz, J. M. Stelmaszyk, A. Constantinescu Crack initiation under thermal fatigue: an overview of CEA experience. Part I: Thermal fatigue appears to be more damaging than uniaxial isothermal fatigue, *Int. J. Fatigue*, 31 (2009), 587–600, doi:10.1016/j.ijfatigue.2008.03.038
- <sup>23</sup> D. Mellouli, N. Haddar, A. Köster, H. F. Ayedi, Hardness effect on thermal fatigue damage of hot-working tool steel, *Engineering Failure Analysis*, 45 (2014), 85–95, doi:10.1016/j.engfailanal.2014.06.007
- <sup>24</sup> J. Absi, J.C. Glandus, Improved methods for severe thermal shocks testing of ceramics by water quenching, *Journal of European Ceramic society*, 24 (2004), 2835–2838, doi:10.1016/j.jeurceramsoc.2003.09.024
- <sup>25</sup> D. Klobčar, J. Tušek, Thermal stresses in aluminium alloy die casting dies, *Comp. Mater. Sci.*, 43 (2008), 1147–1154, doi:10.1016/j.compmat.2008.03.009
- <sup>26</sup> D. Klobčar, J. Tušek, B. Taljat, Thermal fatigue of materials for die-casting tooling, *Mater. Sci. Eng. A*, 472 (2008) 198–207, doi:10.1016/j.msea.2007.03.025
- <sup>27</sup> Y. Birol, Effect of post-oxidation treatment on thermal fatigue behaviour of plasma nitrided hot work tool steel at elevated temperatures, *Surf. Coat. Technol.*, 205 (2010), 597–602, doi:10.1016/j.surfcoat.2010.07.035
- <sup>28</sup> Y. Birol, Response to thermal cycling of duplex-coated hot work tool steels at elevated temperatures, *Mater. Sci. Eng. A*, 528 (2011), 8402–8409, doi:10.1016/j.surfcoat.2010.07.035
- <sup>29</sup> Y. Zhu, D. Schwam, J.F. Wallace, S. Birceanu, Evaluation of soldering, washout and thermal fatigue resistance of advanced metal materials for aluminum die-casting dies, *Mater. Sci. Eng. A*, 379 (2004), 420–31, doi:10.1016/j.msea.2004.03.020
- <sup>30</sup> S. Le Roux, F. Medjedoub, G. Dour, F. Rézaï-Aria, Role of heat-flux density and mechanical loading on the microscopic heat-checking of high temperature tool steels under thermal fatigue experiments, *International Journal of Fatigue*, 51 (2013), 15–25, doi:10.1016/j.ijfatigue.2013.02.004
- <sup>31</sup> M. Wang, Y. Li, Z. Wang, E. Bao, Effect of rare earth elements on the thermal cracking resistance of high speed steel rolls, *Journal of Rare Earths*, 29 (2011) 5, 489–439, doi:10.1016/S1002-0721(10)60485-1
- <sup>32</sup> W. S. Dai, M. Ma, J. H. Chen, The thermal fatigue behavior and cracking characteristics of hot-rolling material, *Materials Science and Engineering A*, 448 (2007), 25–32, doi:10.1016/j.msea.2006.09.003
- <sup>33</sup> Q. C. Jiang, H. L. Sui, Q. F. Guan, Thermal Fatigue Behavior of New Type High Cr Cast Hot Work Die Steel, *ISIJ International*, 44 (2004) 6, 1103–1112, doi:10.2355/isijinternational.44.1103
- <sup>34</sup> Q. C. Jiang, H. Q. Liang, H. L. Sui, Effect of Y Ce Complex Modification on Thermal Fatigue Behavior of High Cr Cast Hot Working Die Steels, *ISIJ International*, 44 (2004) 6, 1762–1781, doi:10.2355/isijinternational.44.1762
- <sup>35</sup> S. Lee, D. H. Kim, J. H. Ryu, K. Shin, Correlation of Microstructure and Thermal Fatigue Property of Three Work Rolls, *Metallurgical and Materials Transaction A*, 28 (1997), 2595–2608, doi:10.1007/s11661-997-0017-6